Numerical modeling of an automated optical belt sorter using the Discrete Element Method

C. Pieper [a,*], G. Maier [b], F. Pfaff [c], H. Kruggel-Emden [a], S. Wirtz [a], R. Gruna [b], B. Noack [c], V. Scherer [a], T. Längle [b], J. Beyerer [b], U.D. Hanebeck [c]

[a] Ruhr-University of Bochum, Universitaetsstrasse 150, 44780 Bochum, Germany
[b] Fraunhofer Institute of Optronics, System Technologies and Image Exploitation, Fraunhoferstrasse 1, 76131 Karlsruhe, Germany
[c] Karlsruhe Institute of Technology, Adenauerring 2, 76131 Karlsruhe, Germany

A B S T R A C T

Optical sorters are important devices in the processing and handling of the globally growing material streams. The precise optical sorting of many bulk solids is still difficult due to the great technical effort necessary for transport and flow control. In this study, particle separation with an automated optical belt sorter is modeled numerically. The Discrete Element Method (DEM) is used to model the sorter and calculate the particle movement as well as particle – particle and particle – wall interactions. The particle ejection stage with air valves is described with the help of a MATLAB script utilizing particle movement information obtained with the DEM. Two models for predicting the particle movement between the detection and separation phase are implemented and compared. In the first model, it is assumed that the particles are moving with belt velocity and without any cross movements and a conventional line scan camera is used for particle detection. In the second model, a more sophisticated approach is employed where the particle motion is predicted with an area scan camera combined with a tracking algorithm. In addition, the influence of different operating parameters like particle shape or conveyor belt length on the separation quality of the system is investigated. Results show that numerical simulations can offer detailed insight into the operation performance of optical sorters and help to optimize operating parameters. The area scan camera approach was found to be superior to the standard line scan camera model in almost all investigated categories.

1. Introduction

The amount of bulk material processed on a global scale continues to grow. In 2012, more than 8687 MT of coal [1] and 2520 MT of grain [2] were produced. The maritime trade of iron ore, grain, coal, bauxite and phosphate increased from 448 MT in 1970 to 3112 MT in 2014 [3]. It is estimated that 10% of the worldwide energy supply is required for the handling and transport of bulk solids [4]. The annual production of bulk materials and powders has a value of over $10 billion and around 25% to 30% of the products produced by the pharmaceutical and chemical industries are particulate solids [5].

With continuously growing material streams, the handling and sorting of bulk solids is of great importance. In addition to conventional separating processes like screens [6], which separate the material depending on physical properties, automated optical sorters can be used. Minerals, agricultural products, granules of recycling processes, or particulate chemical/pharmaceutical substances can be separated based on optical criteria [7–9]. For this purpose, the particulate matter is transported and isolated by chutes, slides or vibrating conveyors and passed by an optical sensor. The bulk solids are then separated into two fractions by pneumatic air valves, which are triggered based on optical properties of the material like size, shape, color, brightness or texture.

Scientific studies conducted in the field of optical sorting can be separated into different core areas. Investigations regarding the sorting of nanoparticles discuss the necessary experimental structures for particle separation and are presented in [10–12]. The main focus regarding the optical sorting of bulk solids is the testing of sorting processes for specific applications. Examples include the separation of magnesite from waste streams [13], the selection of quartz pebbles [14] and the sorting of wheat grains infested with plant disease [15,16]. Other studies investigate the potential of new or modified machine components [8,17–19]. An additional category of research focuses on the applicability of automated optical sorters in new industrial fields or in sub-processes like metal recovery [20], glass recovery [21] or lithium minerals processing [22].

* Corresponding author.
E-mail address: pieper@leat.rub.de (C. Pieper).

Due to the high technical effort necessary for the material transport and flow control, the optical sorting of many bulk solids is still difficult. The gap between particle detection and separation makes it crucial to reduce the proper motion of the bulk solids during transport to be able to reliably predict the particles' position for the material separation. De Jong and Harbeck [23] investigated the maximum throughput of an optical sorter based on different particle sizes. They concluded that the separation efficiency decreases significantly if a minimum distance between adjacent particles is below a certain threshold. Pascoe et al. [24] developed a simple model for predicting the efficiency of their automated sorting system depending on the belt loading and the number of particles to be ejected. In a further study [25], the authors investigated the influence of particle distribution on sorting efficiency with the help of a Monte Carlo simulation.

Due to the heterogeneous nature of bulk solids, the design and calibration of optical sorters is mostly product-specific and highly empirical. The number of air valves required for the material separation and their distance to the optical sensor are currently determined experimentally. Furthermore, the calibration of the valve activation time and the air blast duration is based on simple assumptions (linear particle movement and constant velocity). Hence, adjustments of the system, especially regarding components involved in particle transport and flow control, are based on numerous experiments.

In order to reduce the duration and number of extensive experiments required for the initial calibration of optical sorters, improve sorter accuracy, decrease error probability and enable the optical detection of new particle properties, a new multi-disciplinary approach is employed in this study. It combines digital imaging, algorithmic image processing and numerical simulations. An area scan camera is mounted on an optical belt sorter and enables the real time tracking of the recorded particle stream, giving detailed information of the particles' positions and velocities at the end of the belt. A detailed description of the process can be found in [26,27].

In order to improve the tracking modeling and to get a more detailed understanding of the bulk solid's behavior as well as to improve the design of optical sorters, particle-based simulation approaches like the Discrete Element Method (DEM) can be employed. The DEM has already been successfully applied to describe other material separators like screens [28–31] and cyclones [32–34]. In this study, an optical belt sorter is modeled with the DEM and the influence of different operating parameters like particle shape, applied particle mass and belt length on sorting quality are investigated. The method used to model the complex shaped particles in this study has already been successfully employed and validated against experiments [35,36]. In addition, the results of employing a model of a line scan camera (thereby assuming that the particle is moving in belt direction with belt velocity at the detection point) are compared with using the model of an area scan camera in combination with particle tracking (the actual particle velocity and direction of movement at the detection point are considered). This is a novel approach to optimize sorter performance where the DEM can provide the required insight into particle behavior and sorter parameters.

The particle ejection by air valves is modeled and analyzed with a MATLAB script in a processing step after the simulation. Here, the effects of the number of air valves, air blast duration time and distance between the detection point and the valve bar on the sorting quality are examined. It is planned to model the particle ejection by coupling the DEM with Computational Fluid Dynamics (CFD) in future research, similar to the recently published paper by Fitzpatrick et al. [37]. This study constitutes a first step to numerically model an entire optical sorter, which can be used as a design tool and for further process optimization.

2. Methodology

In this section, the employed DEM approach, the numerical setup and operating parameters as well as the operational procedure are presented.

2.1. DEM approach

The bulk solids and the walls of the optical belt sorter investigated in this study are described with the Discrete Element Method (DEM), first introduced by Cundall and Strack in 1979 [38]. It allows the detailed analysis of particle-particle and particle-wall interactions. The translational and rotational motion of every particle is calculated with Newton's and Euler's equations of motion and can be written as

$$m_i \frac{d^2 \vec{x}_i}{dt^2} = \vec{F}_i^c + \vec{F}_i^g, \tag{1}$$

$$I_i \frac{d\vec{W}_i}{dt} + \vec{W}_i \times \left(I_i \vec{W}_i \right) = \Lambda_i^{-1} \vec{M}_i, \tag{2}$$

where m_i is the particle mass, $d^2\vec{x}_i/dt^2$ the particle acceleration, $\vec{F}_i^c$ the contact force and $\vec{F}_i^g$ is the gravitational force. The second equation gives the angular acceleration $d\vec{W}_i/dt$ as a function of the angular velocity $\vec{W}_i$, the external moment resulting out of contact forces $\vec{M}_i$, the inertia tensor along the principal axis I_i and the rotation matrix converting a vector from the inertial into the body fixed frame Λ_i^{-1}.

The contact forces originating from particle-particle or particle-wall collisions are separated into a normal and tangential component. A linear spring damper model is used to obtain the normal component of the contact force

$$\vec{F}^n = k^n \delta \vec{n} + \gamma^n \vec{v}_{rel}^{\,n}, \tag{3}$$

with the spring stiffness k^n, the virtual overlap δ, the normal vector $\vec{n}$, the damping coefficient γ^n and the normal velocity in the contact point $\vec{v}_{rel}^{\,n}$ [39]. The coefficients of normal restitution between particles e_{pp}^n and particles and walls e_{pw}^n combined with the employed time step directly determine the spring stiffness k^n and the damping coefficient γ^n. A linear spring limited by the Coulomb condition is employed to calculate the tangential component of the contact force

$$\vec{F}^t = \min\left(k^t \left| \vec{\xi}^t \right|, \mu_C \left| \vec{F}^n \right| \right) \vec{t}, \tag{4}$$

where k^t is the stiffness of a linear spring, μ_C is the friction coefficient, $\vec{\xi}^t$ is the relative tangential displacement and $\vec{t}$ is the tangential unit vector [40].

In addition to the tangential contact force, the moments resulting from the rolling friction between particles and particles as well as particles and walls are considered and included in the external moment resulting out of contact forces $\vec{M}_i$ described in Eq. (2). A rolling friction model devised by Zhou et al. [41] is used in this study

$$\vec{M}_i^r = -\mu_r \left| \vec{F}^n \right| \frac{\vec{W}_i}{\left| \vec{W}_i \right|}. \tag{5}$$

Here, μ_r is the coefficient of rolling friction, $\vec{F}^n$ the normal component of the contact force and $\vec{W}_i$ the angular velocity.

The non-spherical particles employed in this study are modeled with polyhedrons. With the help of a triangular surface mesh, different particle shapes can be realized. The contact detection between the polyhedrons is based on a fast common plane algorithm [42]. The contact force laws are equal to those of the spherical particles [39,43].

2.2. Numerical setup and operating parameters

The numerical model considered in this study is based on an actual table-sized, modular optical belt sorter. It combines all major components of a regular full size optical belt sorter with the advantage of being easy to adjust, handle and operate. The system also enables the use of either an area scan camera or a conventional line scan camera for particle detection and localization.

A sketch of the optical belt sorter is shown in Fig. 1. As the system is currently run in a batch operation, the first component of the sorter is a particle container where the bulk solids are located at the beginning of the simulation. Upon the start of the simulation, the container is lifted and the particles are channeled towards the slide by a vibrating feeder which runs at a frequency of 50 Hz and an amplitude of 0.25 mm at a 25° angle. The particles then enter the conveyor belt which has an adjustable length of 0.2 m to 0.6 m, a width of 0.18 m and runs at a constant velocity of 1.5 ms^{-1}.

Components of the sorting process that are not modeled with the DEM are indicated with a dashed box in Fig. 1. The analysis of the sorting quality is conducted with the help of a MATLAB script based on the information on particle motion generated with the DEM. The particle data is processed in the script and a predefined number of air valves is assumed at a predefined distance to the end of the conveyor belt, see Fig. 2. The radius in which the particles are deflected by the compressed air is equal for every nozzle. When employing different nozzle numbers, the radius of these zones is always chosen so that the entire width of the belt is covered. The movement prediction is based on the position and velocity of the particles at the end of the conveyor belt (detection point).

In the case of the line scan camera model, the particle velocity is assumed to be equivalent to that of the conveyor belt and the particle velocity in y-direction is neglected. The valve responsible for the ejection of the detected particle is therefore simply determined by the y-location of the particle. The activation time of the valve is set by calculating the time a particle requires to move from the belt end to the center of the valve bar with the assumption that the particle has constant belt velocity in x-direction.

In the case of the area scan camera model, the assumption is made that both the x- and y-velocity of every particle are known at the end of the conveyor belt, due to the applied particle tracking. Consequently, the valve responsible for particle ejection is determined based on the location of the particle at the belt end and the additional movement in y-direction depending on the y-velocity of the particle. The activation time of the valve is also set by calculating the time a particle needs to move from the belt end to the center of the valve bar, but the actual particle velocity in x-direction is considered.

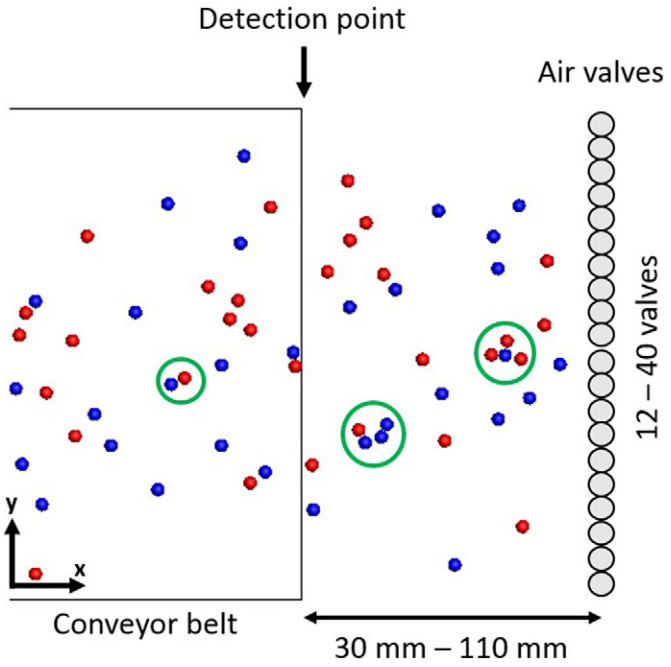

Fig. 2. Sketch of the air valve implementation within MATLAB.

The duration in which the valves release the jets of compressed air can also be adjusted in the MATLAB script. Here the assumption is made that only particles whose center of gravity lies within the valve air influence zone during the activation timeframe are considered as ejected. This simplification is made under the consideration that the particle sizes of the different particle shapes are very similar.

Three different particle shapes are employed in this study, namely spheres, cylinders and plates. Their material parameters, which are also required for the DEM simulations, are based on beech wood particles [44] and are presented in Table 1. The coefficients of normal

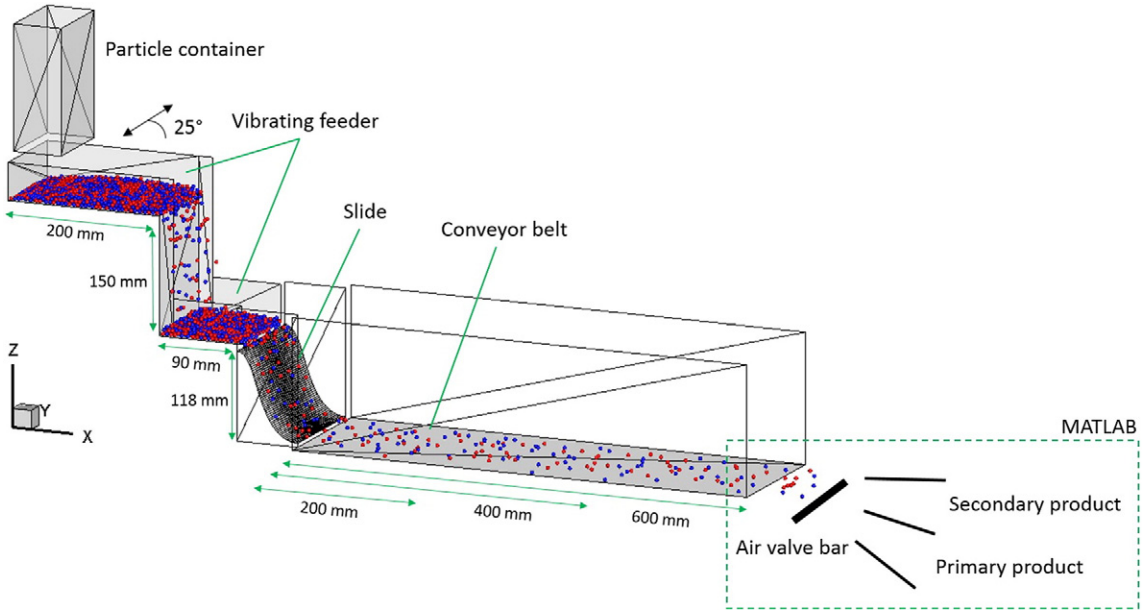

Fig. 1. Sketch of the optical belt sorter modeled with the DEM.

Table. 1
Particle properties required for the DEM simulation including size, volume, density ρ_p, coefficient of restitution between particles e^n_{pp}, particles and belt $e^n_{pw\_belt}$, particles and sorter walls $e^n_{pw\_sorter}$, Coulomb friction coefficient between particles $\mu^n_{c\_pp}$, particles and belt $\mu^n_{c\_pw\_belt}$, particles and sorter walls $\mu^n_{c\_pw\_sorter}$ and the rolling friction coefficient between particles and belt μ_r as well as the contact stiffness of the linear spring k^n and k^t and the damping coefficient γ^n.

Shape	Sphere	Cylinder	Plate
			
Size [mm]	5	3 × 9	2 × 5 × 6
Volume [mm^3]	65.450	60.590	61.561
ρ_p [kg/m^3]	823.0	754.4	754.1
e^n_{pp} [−]	0.5	0.5	0.5
$e^n_{pw\_belt}$ [−]	0.55	0.55	0.55
$e^n_{pw\_sorter}$ [−]	0.55	0.55	0.55
$\mu^n_{c\_pp}$ [−]	0.4	0.4	0.4
$\mu^n_{c\_pw\_belt}$ [−]	0.16	0.16	0.16
$\mu^n_{c\_pw\_sorter}$ [−]	0.25	0.25	0.25
μ_r [−]	$1.01 \cdot 10^{-4}$	$1.01 \cdot 10^{-4}$	–
k^n [kg/s^2]	4460.07	3740.49	3800.43
k^t [kg/s^2]	3780.09	3170.22	3221.03
γ^n [kg/s]	0.1493	0.1253	0.1273

restitution, Coulomb friction and rolling friction were determined experimentally according to the procedures described by Höhner et al. [45] and Sudbrock et al. [46]. The rolling friction coefficient was investigated for the particle-belt interaction. Alteration of the parameter between particles and sorter walls was found to have negligible effects on the particle behavior. To assess the importance of the selected DEM parameters, a sensitivity analysis is conducted and evaluated in this study. The DEM simulations are performed with a time step of $1 \cdot 10^{-5}$ s. A maximum particle overlap of 0.5% is ensured. The spring stiffness k^n and k^t as well as the damping coefficient γ^n are calculated from the chosen time step and the coefficient of restitution.

2.3. Operational procedure

In order to compare the sorting quality results of the line scan camera with those obtained using the area scan camera model, a base case is defined and six operating parameters are altered one at a time in different simulation series. These are presented in Table 2. The highlighted values form the base case of the study. In addition to the presented simulation series, a sensitivity analysis of important DEM parameters is conducted.

Three of the parameters are adjusted in the MATLAB script. These include the overall quantity of the valves used for sorting, their activation duration and the distance of the valve bar from the detection point, namely the conveyor belt end. The parameters examined on the DEM side include the applied particle mass, conveyor belt length and particle shape. As the variation of the operating parameters on the MATLAB side requires significantly less calculation time compared to the DEM simulations, more values were tested. The introduced particle stream always consists of equal portions of red and blue particles, meaning that 50% of the bulk solids have to be separated. The target particles are always the blue bulk solids. The initial particle packing within the particle container (see Fig. 1) is generated randomly at the beginning of each simulation. The red and blue particles are perfectly mixed. Before the container is moved upwards, thereby releasing the particles onto the vibrating feeder, the particles settle under gravity and form a loose packing.

Table. 2
Investigated operational parameters on the MATLAB and DEM side.

Parameter	MATLAB			Discrete Element Method		
	Valve quantity [–]	Valve activation duration [s]	Valve bar distance [m]	Introduced particle mass [kg]	Conveyor belt length [m]	Particle shape [–]
	12	0.0025	0.03	0.1	0.2	Cylinders
	16	0.004	0.05	0.2	0.4	Spheres
	20	0.005	0.07	0.3	0.6	Plates
	24	0.01	0.09			
	28	0.015	0.1			
	32	0.02	0.11			
	36					
	40					

3. Results and discussion

In this section, the obtained results are presented and discussed. First, an initial validation of the particle behavior on the conveyor belt is provided, followed by a discussion of the conducted numerical investigation. A sensitivity analysis of important DEM parameters concludes this section.

3.1. Initial validation of conducted simulations

In order to confirm the qualitative accuracy of the conducted simulations, the average particle velocity on the conveyor belt is compared between the simulations and corresponding experiments carried out on the modular optical belt sorter. As the main focus of this study is based on the particle movement on the belt, this component of the sorter was considered the most crucial. The base case of the study as well as the cylinder and plate case are investigated.

The conveyor belt is separated into four equal parts, each 0.1 m in length. In every section, the average particle velocity is detected, for both the simulation and experiment. The velocity of the conveyor belt is set to 1.15 ms^{-1} as this was the initially investigated belt velocity. The other system parameters are equivalent to the base case of the study.

During the experiments, the particle movement on the conveyor belt is recorded with a high speed camera in each investigated section. A tracking algorithm [26] is then applied on the particle data obtained by the recorded visual material, providing detailed information on the particle velocity in the respective belt section. The obtained values for every particle are then averaged. For the simulation the average particle velocities in the different belt sections can easily be calculated in a post processing step, providing comparable results to those received from the experiments. The standard deviation of the calculated average particle velocities, based on the velocity variation of the individual particles, is also given.

The results obtained by the sphere analysis can be seen in Fig. 3. The figure shows that the average sphere velocity initially increases to values higher than the belt velocity for both the simulation and the experiment, due to the particle acceleration induced by the slide. At the end of the conveyor belt, the particle velocity has started to decrease in both cases. Here, the general trend of the particle movement shows good agreement between experiment and simulation. At the start of

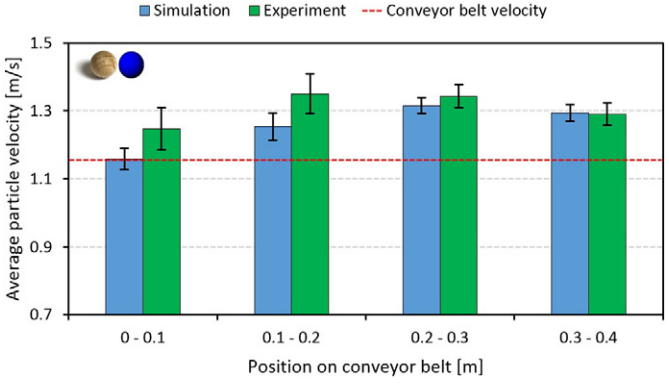

Fig. 3. Average particle velocity of spheres in belt direction compared between simulation and experiment.

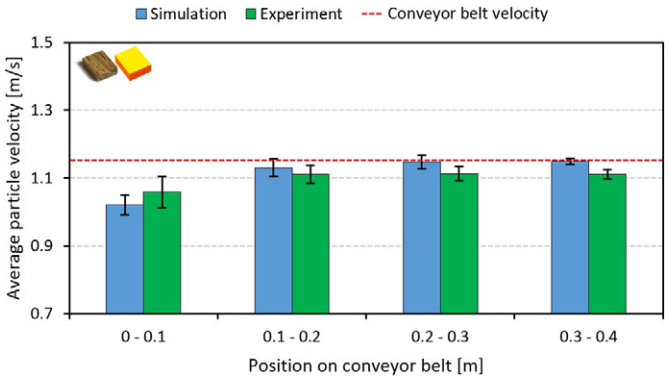

Fig. 4. Average particle velocity of plates in belt direction compared between simulation and experiment.

the belt, the average particle velocities obtained by the experiments are slightly higher compared to the simulation. This is most likely related to small discrepancies of the feed system. However, the results show that experiment and simulation show very good agreement, especially considering the second half of the conveyor belt, which is most important for the investigations performed in this study. As expected, the standard deviation of the velocities obtained by the experiments are higher compared to those of the simulation, as there is always a marginal number of false track associations or visual impurities that are considered as particles [26]. In both simulation and experiment the standard deviation decreases with rising belt length.

The results of the plate case is presented in Fig. 4. Here, the particles enter the conveyor belt at a much lower average velocity and continue to converge towards the belt velocity over the length of the belt. The velocity development of the simulation and experiment are in good agreement and only show slight differences. In the simulation, the average velocity of the plates is closer to the conveyor belt velocity compared to the experimental findings.

The average particle velocities of cylinders for both experiments and simulations are shown in Fig. 5. The results are very similar to the plate case. The particle velocity of the cylinders increases at the start of the belt and continues to rise towards the velocity of the belt for both the simulation and experiment. Again, the simulated particles show a higher tendency to adapt to the conveyor belt velocity.

3.2. Numerical investigations

Two main indicators for separation quality are analyzed for each conducted simulation series. The first is the percentage of particles that are not ejected by the air valves even though they should have been separated from the material stream. The second indicator shows the percentage of particles falsely co-ejected by the air valves as so

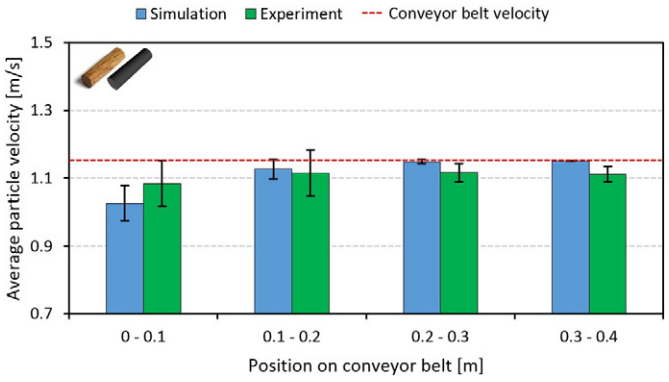

Fig. 5. Average particle velocity of cylinders in belt direction compared between simulation and experiment.

called "by-catch". To ensure a clear visual separation of the two categories, the not ejected particle indicator is plotted in dashed lines and the falsely co-ejected indicator in filled ones. In both categories, the separation results of the line scan camera and the area scan camera model in combination with the particle tracking are compared. In addition, the results achieved under perfect separation conditions (using the exact particle positions modeled within the DEM for valve activation) are presented.

The separation quality of the base case can be seen in Fig. 6. To measure the impact of different initial particle configurations on the calculated results, the DEM simulation of the base case was performed and evaluated three times. The initial particle packing was randomly generated at the start of each simulation. Average values as well as the standard deviation obtained from the simulations are depicted in Fig. 6.

The results show that the number of particles not ejected when employing the line scan camera model is significantly higher compared with the area scan camera model, which demonstrates how important detailed knowledge of the particles' motion is to obtain a good separation quality. Under ideal conditions (dashed red line) all particles are obviously ejected. The differences between the falsely ejected particle results are not as distinct. About 8% to 9% of the particles are ejected as by-catch. Nevertheless, when applying the line scan camera model, the number of falsely ejected particles is slightly lower compared to the results of the area scan camera model and under perfect separation, due to the formation of particle clusters on the conveyor belt, marked with green circles in Fig. 2. When only a fraction of the particles within such clusters is supposed to be ejected, the others are deflected as well. As the separation quality of the line scan camera model is significantly lower compared to the area scan camera model, some of these particle clusters are not ejected, which then also leads to a reduction in falsely co-ejected particles.

The standard deviations of the different investigated categories are all below 4%. Only for the area scan camera model a slightly higher value is obtained. This is not surprising, however, due to the fact that at these low particle ejection percentages, a difference of a few deflected particles already has a high impact. As the results and the derived conclusions in this study are of a qualitative nature and the deviations between the different simulation series are very small, only one simulation is conducted for every altered parameter. This greatly reduces the required calculation time with negligible effects on the obtained results.

3.2.1. Influence of air valve number

The first operating parameter investigated in this study is the influence of the number of air valves employed. Starting with only 12 valves, the number is increased gradually at four valve increments up to 40

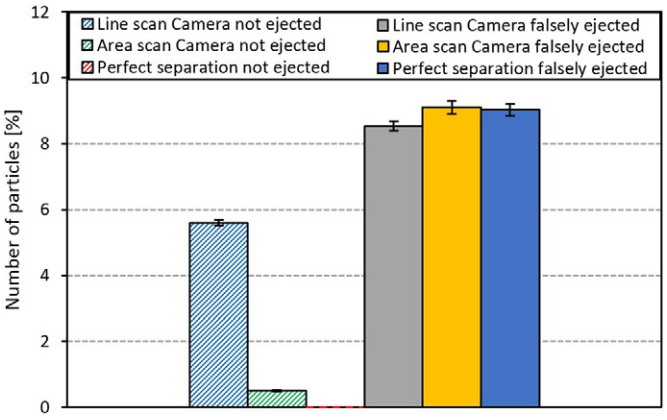

Fig. 6. Average separation quality of the base case (20 air valves, 0.01 s activation duration, 0.07 m distance, 0.2 kg of particles, 0.4 m belt length and spheres).

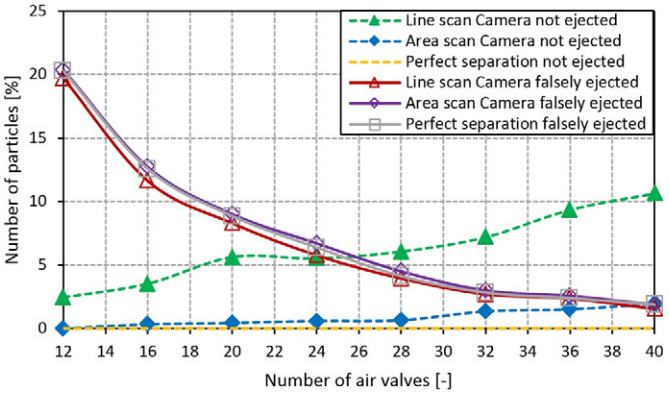

Fig. 7. Separation quality depending on the number of employed air valves.

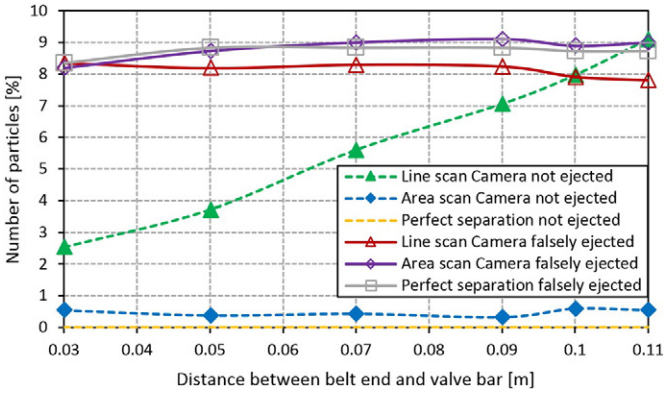

Fig. 9. Separation quality depending on the distance between belt end and valve bar.

valves, resulting in an influence zone ranging from a radius of 0.75 cm to 0.225 cm. The results are presented in Fig. 7.

The graph shows that the percentage of not ejected particles continuously increases with a rising number of air valves, both for the line and area scan camera model. The number of falsely co-ejected particles decreases with rising valve numbers in all three evaluation models. As the air influence radius is significantly reduced with growing valve quantity, a precise prediction of the particle position at the ejection stage becomes increasingly important. As to be expected, the likelihood of not ejecting a particle that should be separated from the material stream is higher when the valve influence area is smaller. The importance of exact particle motion prediction is underlined when comparing the line and area scan camera results. While the number of not ejected particles increases by a margin of about 2% for 40 valves with the area scan camera model, the percentage of not ejected particles increases by a margin of around 8% when employing the line scan camera approach. The falsely co-ejected particle number decreases from about 20% for 12 valves to 2% for 40 valves and is very similar for all investigated models. As the influence radius of the valves is greatly reduced, less particles are falsely co-ejected. At the lower valve quantity numbers the percentage of falsely ejected particles of the line scan camera model is slightly lower compared to the other two models. This can be explained by the particle cluster formation discussed in the previous section. At higher valve numbers, this difference disappears due to the very small air influence radius. Even if particles are clustered, they are no longer always deflected as an entity.

3.2.2. Influence of valve activation duration

The second examined operating parameter is the valve activation duration. Results for durations ranging from 0.0025 s to 0.02 s are shown in Fig. 8.

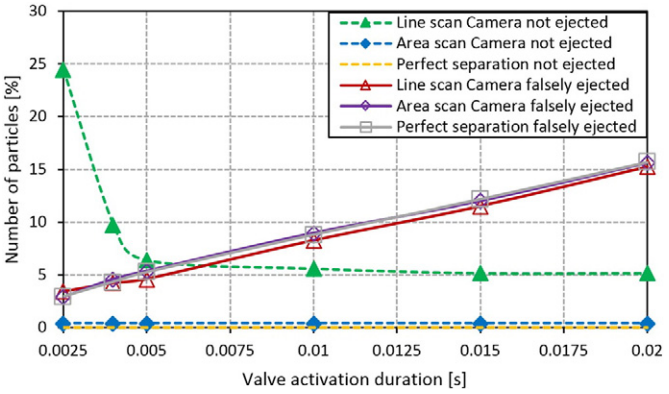

Fig. 8. Separation quality depending on the valve activation duration.

When applying the line scan camera model the percentage of not ejected particles starts at a value of 24.5% at a duration of 0.0025 s and then quickly drops to a value of around 5.5% for 0.01 s. From there, the curve remains fairly constant. In contrast to this, the results of the area scan camera remain unchanged at a low value of about 0.5%. The curve of the line scan camera suggests that 5% of the not ejected particles are falsely predicted by neglecting the particle velocity in y-direction. During the very short air blast intervals of 0.0025 s to 0.004 s, only a precise velocity prediction in x-direction ensures a good sorting quality. The number of falsely co-ejected particles increases almost linearly with rising valve activation durations. The values of the line scan camera are again slightly lower compared to the other two analyzed models. Operating an automated optical sorter with low activation durations and therefore low by-catch and maintaining a good sorting quality seems only possible when employing a precise prediction tool like the area scan model presented in this study.

3.2.3. Influence of distance between belt end and valve bar

The third operating parameter investigated is the distance between the belt end, which is also the particle detection point, and the valve bar. The findings are presented in Fig. 9.

The ratio of not ejected particles rises steadily with increasing distance between belt end and valve bar when employing the line scan camera model. In contrast, the number of not ejected particles remains fairly constant at a much lower value when using the area scan camera model. With a larger gap between detection and separation point, the need for a precise motion prediction increases. If the particle velocity is not predicted accurately enough, the spatial offset from the expected location, once the particle reaches the valve bar prevents a good separation result. The number of falsely co-ejected particles remains relatively equal at a value between 8% and 9%. Again, the values of the line scan camera model are slightly lower compared to the other two approaches

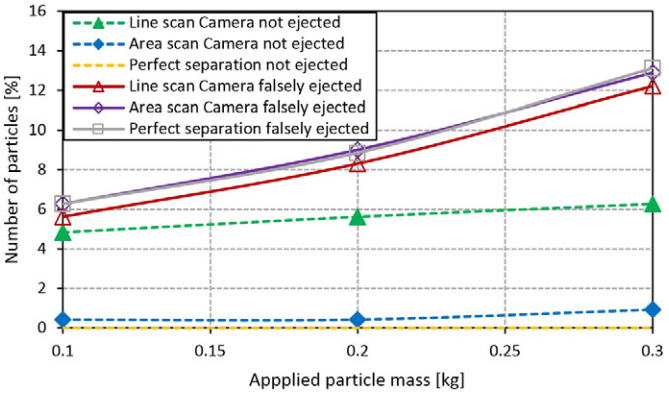

Fig. 10. Separation quality depending on the applied particle mass.

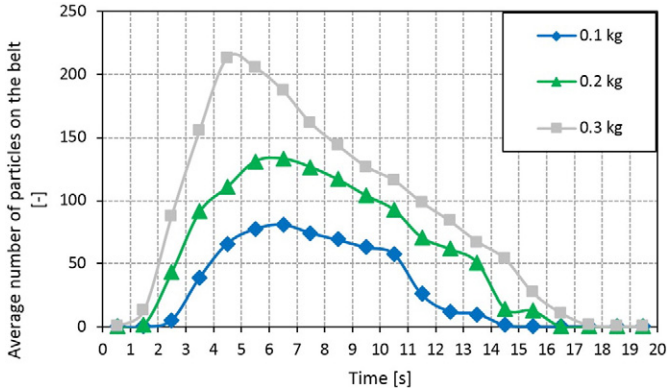

Fig. 11. Average number of particles on the conveyor belt plotted against time.

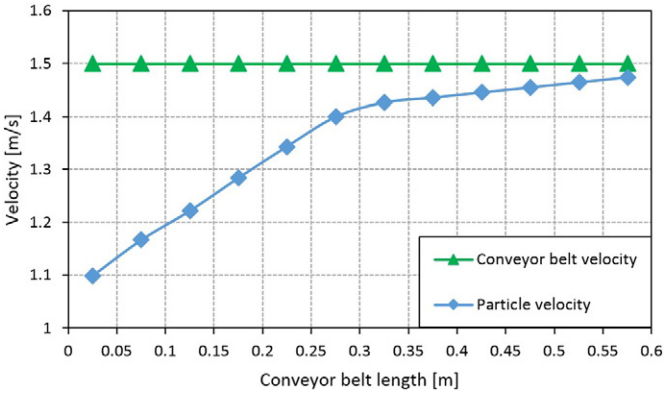

Fig. 13. Average particle velocity plotted against the conveyor belt length.

and the offset increases with higher differences between the not ejected particles of the line and area scan camera model. Small fluctuations are most likely the result of situational occurrences in the particle stream.

3.2.4. Influence of applied particle mass

The fourth operating parameter investigated and altered for the DEM simulation is the applied mass of the entire particle packing, where 0.1 kg, 0.2 kg and 0.3 kg are examined. Results are depicted in Fig. 10.

The graph shows that both the percentage of not ejected and falsely co-ejected particles rises with increasing applied particle mass. A higher throughput causes increased particle interaction and therefore a higher likelihood of orthogonal or irregular particle movement. The results match the experimental findings of Udoudo [47]. The differences in belt loading, when applying varying initial particle masses, can be seen in Fig. 11. In comparison to the area scan camera model, the number of not ejected particles is again significantly higher when utilizing the line scan camera approach. Similar to previous observations, the number of falsely co-ejected particles of the line scan camera is slightly lower compared to the other models.

3.2.5. Influence of conveyor belt length

The influence of the conveyor belt length is also modeled within the DEM. A length of 0.2 m, 0.4 m and 0.6 m is evaluated. The findings are presented in Fig. 12.

The results show that the line scan camera model has a very high percentage of about 40% of not ejected particles at a short belt length of 0.2 m. As the model is based on the simple assumption that the particles have reached belt velocity at the detection point and only move in belt direction, the particle position at the separation stage is not predicted accurately enough. The particles have not adapted to the belt velocity and orthogonal movement to the belt direction is still high. This can be seen in Fig. 13. The graph shows the average particle velocity in belt direction, depending on the position on the conveyor belt.

At a length of 0.4 m, the number of not ejected particles of the line scan camera model has already declined to about 5% and for a length of 0.6 m to about 2%. The model of the area scan camera assesses the actual particle velocity in x- and y-direction and is therefore capable of accurately predicting the position at the separation point even at a low belt length. The percentage of particles not ejected by the valves remains at a constant low of about 0.5%. The number of falsely co-ejected particles is very similar for all three models and stays fairly constant at values between 8% and 9%.

3.2.6. Influence of particle shape

The effect of different particle shapes on the separation quality is investigated in the final simulation series. Cylinders, spheres and plates (described in detail in Section 2.2) are considered. The corresponding results are presented in Fig. 14.

The percentages of particles not ejected by the air valves of cylinders and spheres are very similar with values of about 5.6% for the line scan camera model. The number of not ejected particles when employing plates is considerably lower. In contrast to the cylinders and spheres the plates show no rolling motion once they are on the conveyor belt, which greatly reduces particle movement orthogonal to the belt direction. In comparison to the line scan camera model, the percentages of not ejected particles based on the area scan camera model are significantly lower for all investigated particle shapes.

The number of falsely co-ejected particles is slightly different for each of the particle shapes. Cylinders have the highest percentage followed by plates and lastly spheres. These differences are probably related to different particle feed rates between the investigated particle shapes. Both aspects affect the particle proximity which directly

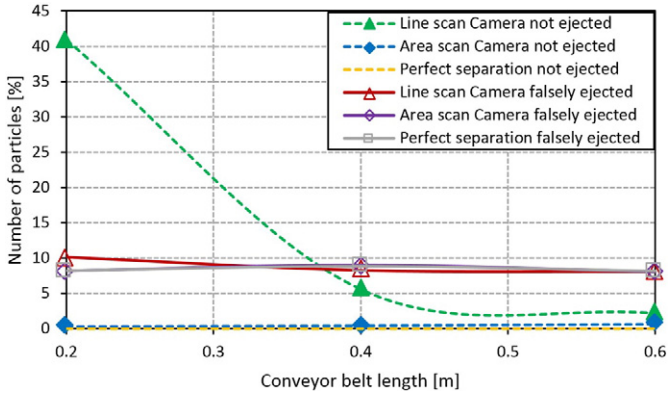

Fig. 12. Separation quality depending on the conveyor belt length.

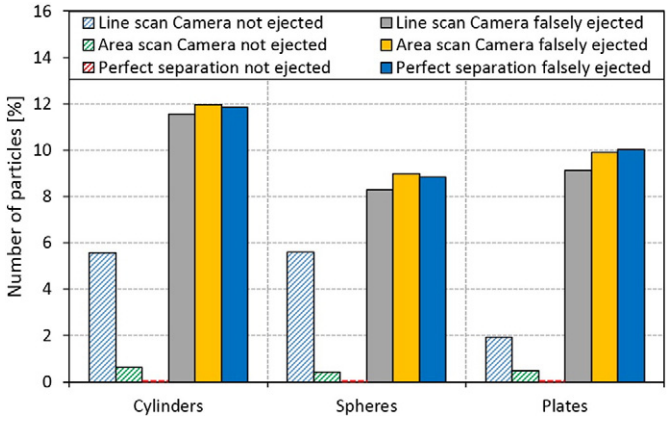

Fig. 14. Separation quality depending on the particle shape.

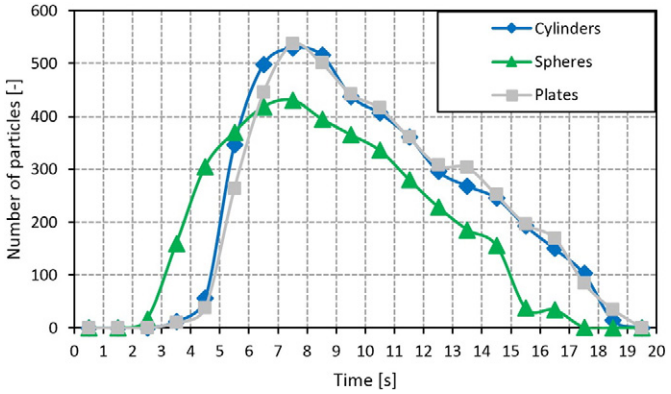

Fig. 15. Number of particles entering the belt plotted against time.

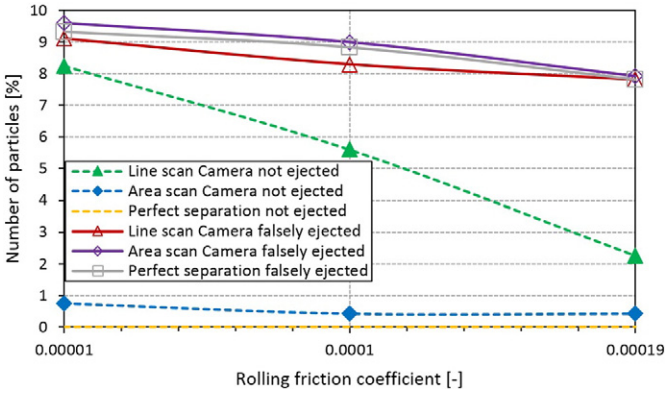

Fig. 16. Separation quality depending on the coefficient of rolling friction between particles and conveyor belt.

influences the rate of falsely co-ejected particles as discussed in Section 3.2.4. The number of particles entering the conveyor belt during the simulation is depicted in Fig. 15. The figure shows that the spheres enter the conveyor belt at a much more uniform rate compared to cylinders and plates. This entails that fewer particles are transported by the belt at the same time, thereby reducing the number of falsely co-ejected particles.

A comparison between the applied prediction models shows that spheres and cylinders have very similar results. In both cases, the percentage of co-ejected particles of the line scan camera model is lower compared to the other two approaches due to the much higher number of not ejected particles. This is different for plates. Here the line scan camera model has the highest percentage of co-ejected particles. This is probably explained by the fact that the difference between the number of not ejected particles between the line and area scan camera is not as high.

It is important to consider that the particle shape only influences the particle behavior on the conveyor belt and the particle-particle and particle-wall interactions. As only the center of gravity is currently considered for particle ejection, the shape has no influence on the separation phase itself. This aspect will be thoroughly investigated when using CFD for particle ejection and thereby accurately modeling the entire valve.

3.3. Sensitivity analysis of DEM parameters

In order to understand the impact of choosing the correct material parameters for the conducted DEM simulations, the influence of the coefficient of rolling friction and Coulomb friction on sorting quality is assessed in a sensitivity analysis. On the basis of the experimentally obtained values, a higher and lower coefficient is additionally employed. The base case of the study is used for the alterations.

The results of utilizing different rolling friction coefficients between the particles and the conveyor belt are presented in Fig. 16. The graph shows that the number of not ejected and falsely co-ejected particles decreases with a rising rolling friction coefficient in all investigated prediction models. A higher rolling friction coefficient leads to a reduction in cross movement of the particles and the bulk solids adapt the belt velocity at a much faster rate. The number of not ejected particles is significantly higher for the line scan camera model compared to the area scan camera approach.

The impact on sorting quality when different Coulomb friction coefficients are employed can be seen in Fig. 17. At low Coulomb friction coefficients, the number of not ejected particles is very high for the line scan camera approach, as the particles are less inclined to follow the conveyor belt velocity or direction, leading to wrong ejection predictions. The model employing the area scan camera is almost unaffected by the change in friction coefficient. The number of falsely ejected particles only shows a slight increase with rising friction coefficients for all investigated models.

The sensitivity analysis shows that employing different friction coefficients can have a significant impact on sorting quality, especially regarding the line scan camera model. However, the qualitative result, namely that the model combining an area scan camera with particle tracking is superior to the convectional line scan camera model, remains true for all investigated friction coefficients.

4. Conclusions

A numerical model of an automated optical belt sorter based on the Discrete Element Method in combination with a MATLAB script for particle ejection was described and analyzed in this study. Two models for particle detection and movement prediction, namely a line scan camera (assuming that the particle has reached belt velocity at the detection point and neglecting possible particle movement in y-direction) and an area scan camera model with subsequent particle tracking (considering the actual particle velocity in x- and y-direction at the detection point), were presented and compared. Different operating parameters of the optical sorter were altered one at a time and the resulting influence on sorting quality was assessed. The following conclusions can be drawn from this study:

- The employed model of the area scan camera with combined particle tracking is superior to the conventional line scan camera model in all investigated operation modes. Merely the number of falsely co-ejected particles is often slightly higher, which can be attributed to the formation of particle clusters. The qualitative results are in agreement with the findings of Pfaff et al. [26].

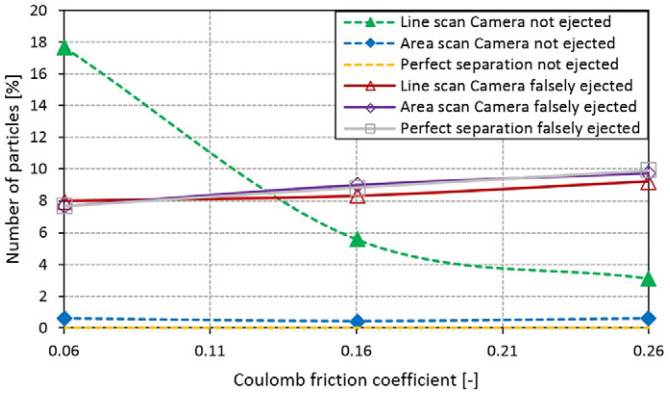

Fig. 17. Separation quality depending on the Coulomb friction coefficient between particles and conveyor belt.

- Employing a higher number of air valves for the separation stage can help reduce the percentage of falsely co-ejected particles. However, the accurate prediction of particle motion is crucial to prevent a significant rise in the number of not ejected particles. High valve activation durations ensure that the number of not ejected particles is very low, at the cost of higher by-catch rates. Larger distances between the detection and separation phase directly lead to a linear increase in the percentage of not ejected particles when employing the line scan camera model. Falsely co-ejected particle numbers remain relatively unaffected. In all investigated cases regarding the separation stage of the sorter, optimized detection and prediction methods like the area scan camera approach can offer the required precision to achieve accurate particle separation with low particle by-catch.
- As expected, increasing the applied particle mass leads to a reduction in overall sorting quality of the optical sorter. This is in line with the results of Pascoe et al. [24] and Udoudo [47]. Reducing the conveyor belt length only negatively effects the sorting quality of the line scan camera model. Shorter and therefore more economical belts can be utilized when applying a more sophisticated prediction approach. The particle shape greatly influences particle movement on the conveyor belt and therefore directly effects the sorting efficiency. Plates show significantly lower cross movements and adapt to the belt velocity much faster compared to spheres and cylinders, making it easier to accurately predict their motion. These particle characteristics can also be transferred to industrial bulk solids.
- The investigation showed that numerical simulations of optical sorters can help to optimize operating parameters according to the desired application. Depending on the sorter adjustments, the emphasis can be laid on reducing the number of not ejected particles or the percentage of falsely co-ejected bulk solids.

The study provides a first step towards modeling an entire automated optical belt sorter. For future improvement, the separation step needs to be analyzed and described in greater detail. Here the coupling of DEM with CFD can provide the necessary insight. Although an initial comparison between simulation and experiment has been conducted, the presented numerical results and observations are of qualitative nature and still require additional verification by corresponding experiments. It is also planned to model and investigate industrial bulk solids like coffee beans, glass shards or peppercorns with the DEM.

Acknowledgements

The IGF project 18798 N of the research association Forschungs-Gesellschaft Verfahrens-Technik e.V. (GVT) was supported via the AiF in a program to promote the Industrial Community Research and Development (IGF) by the Federal Ministry for Economic Affairs and Energy on the basis of a resolution of the German Bundestag.

References

[1] U.S. Energy Information Administration, Total Primary Coal Production, 2016 (https://www.eia.gov/cfapps/ipdbproject/IEDIndex3.cfm?tid=1&pid=7&aid=1).
[2] Food and Agriculture Organization of the United Nation, Fao Statistical Yearbook 2013 - World Food and Agriculture, 2013 http://dx.doi.org/10.1088/1751-8113/44/8/085201.
[3] Review of Maritime Transport, 2015, United Nations Publications, 2015.
[4] J. Duran, Sands, Powders, and Grains, Springer New York, New York, NY, 2000 http://dx.doi.org/10.1007/978-1-4612-0499-2.
[5] D. McGlichey, Characterisation of Bulk Solids, Blackwell Publishing Ltd., Oxford, UK, 2005 http://dx.doi.org/10.1002/9781444305456.
[6] M. Stieß, Mechanische Verfahrenstechnik 1, Springer, Berlin Heidelberg, Berlin, Heidelberg, 1995 http://dx.doi.org/10.1007/978-3-662-08600-1.
[7] M. Graves, B. Batchelor, Machine Vision for the Inspection of Natural Products, Springer, 2004 http://dx.doi.org/10.1007/s13398-014-0173-7.2.
[8] M.D. Wedel, Optische Sortierung von mineralischen Rohstoffen, Schüttgut 10 (2004) 212–216.
[9] T. Pearson, D. Brabec, S. Haley, Color image based sorter for separating red and white wheat, Sens. & Instrumen. Food Qual. 2 (2008) 280–288, http://dx.doi.org/10.1007/s11694-008-9062-0.
[10] M. Ploschner, T. Čižmár, M. Mazilu, A. Di Falco, K. Dholakia, Bidirectional optical sorting of gold nanoparticles, Nano Lett. 12 (2012) 1923–1927, http://dx.doi.org/10.1021/nl204378r.
[11] I. Perch-Nielsen, D. Palima, J.S. Dam, J. Glückstad, Parallel particle identification and separation for active optical sorting, J. Opt. A Pure Appl. Opt. 11 (2009) 034013, http://dx.doi.org/10.1088/1464-4258/11/3/034013.
[12] B. Ma, B. Yao, F. Peng, S. Yan, M. Lei, R. Rupp, Optical sorting of particles by dual-channel line optical tweezers, J. Opt. 14 (2012) 105702, http://dx.doi.org/10.1088/2040-8978/14/10/105702.
[13] K. Bilir, H. Akdas, Evaluation of Magnesite Wastes Using Optical Sorting Machine, 1997 7.
[14] D.M. Dehler, Optische Sortierung von Quarzkieseln zur Senkung des Eisengehaltes, Aufbereitungstechnik 47 (2006) 6–8.
[15] S.R. Delwiche, T.C. Pearson, D.L. Brabec, High-speed optical sorting of soft wheat for reduction of deoxynivalenol, Plant Dis. 89 (2005) 1214–1219, http://dx.doi.org/10.1094/PD-89-1214.
[16] F.E. Dowell, T.N. Boratynski, R.E. Ykema, A.K. Dowdy, R.T. Staten, Use of optical sorting to detect wheat kernels infected with *Tilletia indica*, Plant Dis. 86 (2011) 500–502.
[17] M. Dehler, Optical sorting of ceramic raw material, T. 19 (2003) 248–251.
[18] G. Ligus, Municipal waste management model with the use of optical sorting elements, Chemik. 66 (2012) 1229–1234.
[19] H.R. Manouchehri, Sorting: possibilities, limitations and future, Proc. Miner. Process. (2003).
[20] M. Bigum, L. Brogaard, T.H. Christensen, Metal recovery from high-grade WEEE: a life cycle assessment, J. Hazard. Mater. 207–208 (2012) 8–14, http://dx.doi.org/10.1016/j.jhazmat.2011.10.001.
[21] N. Dias, M. Teresa Carvalho, P. Pina, Characterization of mechanical biological treatment reject aiming at packaging glass recovery for recycling, Miner. Eng. 29 (2012) 72–76, http://dx.doi.org/10.1016/j.mineng.2011.10.004.
[22] F. Brandt, R. Haus, New concepts for lithium minerals processing, Miner. Eng. 23 (2010) 659–661, http://dx.doi.org/10.1016/j.mineng.2010.03.021.
[23] De Jong, T.P.R. Harbeck, Automated sorting of minerals: current status and future outlookProc. 37th Can. Miner. Process. Conf. 2005, pp. 629–648.
[24] R.D. Pascoe, O.B. Udoudo, H.J. Glass, Efficiency of automated sorter performance based on particle proximity information, Miner. Eng. 23 (2010) 806–812, http://dx.doi.org/10.1016/j.mineng.2010.05.021.
[25] R.D. Pascoe, R. Fitzpatrick, J.R. Garratt, Prediction of automated sorter performance utilising a Monte Carlo simulation of feed characteristics, Miner. Eng. 72 (2015) 101–107, http://dx.doi.org/10.1016/j.mineng.2014.12.026.
[26] F. Pfaff, M. Baum, B. Noack, U.D. Hanebeck, R. Gruna, T. Langle, et al., TrackSort: predictive tracking for sorting uncooperative bulk materials, IEEE Int. Conf. Multisens. Fusion Integr. Intell. Syst. 2015-Octob 2015, pp. 7–12, http://dx.doi.org/10.1109/MFI.2015.7295737.
[27] F. Pfaff, C. Pieper, G. Maier, B. Noack, H. Kruggel-emden, R. Gruna, et al., Improving Optical Sorting of Bulk Materials Using Sophisticated Motion Models, 2015 http://dx.doi.org/10.1515/teme-2015-0108.
[28] P.W. Cleary, M.D. Sinnott, R.D. Morrison, Separation performance of double deck banana screens - part 1: flow and separation for different accelerations, Miner. Eng. 22 (2009) 1218–1229, http://dx.doi.org/10.1016/j.mineng.2009.07.002.
[29] K.J. Dong, A.B. Yu, I. Brake, DEM simulation of particle flow on a multi-deck banana screen, Miner. Eng. 22 (2009) 910–920, http://dx.doi.org/10.1016/j.mineng.2009.03.021.
[30] J. Xiao, X. Tong, Characteristics and efficiency of a new vibrating screen with a swing trace, Particuology 11 (2013) 601–606, http://dx.doi.org/10.1016/j.partic.2012.07.014.
[31] Z. Li, X. Tong, A study of particles penetration in sieving process on a linear vibration screen, Int. J. Coal Sci. Technol. 2 (2015) 299–305, http://dx.doi.org/10.1007/s40789-015-0089-7.
[32] K.W. Chu, B. Wang, D.L. Xu, Y.X. Chen, A.B. Yu, CFD-DEM simulation of the gas-solid flow in a cyclone separator, Chem. Eng. Sci. 66 (2011) 834–847, http://dx.doi.org/10.1016/j.ces.2010.11.026.
[33] K.W. Chu, B. Wang, A.B. Yu, A. Vince, G.D. Barnett, P.J. Barnett, CFD-DEM study of the effect of particle density distribution on the multiphase flow and performance of dense medium cyclone, Miner. Eng. 22 (2009) 893–909, http://dx.doi.org/10.1016/j.mineng.2009.04.008.
[34] K.W. Chu, B. Wang, A.B. Yu, A. Vince, CFD-DEM modelling of multiphase flow in dense medium cyclones, Powder Technol. 193 (2009) 235–247, http://dx.doi.org/10.1016/j.powtec.2009.03.015.
[35] H. Kruggel-Emden, T. Oschmann, Numerical study of rope formation and dispersion of non-spherical particles during pneumatic conveying in a pipe bend, Powder Technol. 268 (2014) 219–236, http://dx.doi.org/10.1016/j.powtec.2014.08.033.
[36] K. Vollmari, T. Oschmann, S. Wirtz, Pressure drop investigations in packings of arbitrary shaped particles, Powder Technol. 271 (2015) 109–124, http://dx.doi.org/10.1016/j.powtec.2014.11.001.
[37] R.S. Fitzpatrick, H.J. Glass, R.D. Pascoe, CFD–DEM modelling of particle ejection by a sensor-based automated sorter, Miner. Eng. 79 (2015) 176–184, http://dx.doi.org/10.1016/j.mineng.2015.06.009.
[38] P.A. Cundall, O.D.L. Strack, A discrete numerical model for granular assemblies, Géotechnique 29 (1979) 47–65, http://dx.doi.org/10.1680/geot.1980.30.3.331.
[39] H. Kruggel-Emden, E. Simsek, S. Rickelt, S. Wirtz, V. Scherer, Review and extension of normal force models for the discrete element method, Powder Technol. 171 (2007) 157–173, http://dx.doi.org/10.1016/j.powtec.2006.10.004.
[40] H. Kruggel-Emden, S. Wirtz, V. Scherer, A study on tangential force laws applicable to the discrete element method (DEM) for materials with viscoelastic or plastic behavior, Chem. Eng. Sci. 63 (2008) 1523–1541, http://dx.doi.org/10.1016/j.ces.2007.11.025.

[41] Y.C. Zhou, B.D. Wright, R.Y. Yang, B.H. Xu, A.B. Yu, Rolling friction in the dynamic simulation of sandpile formation, Physica A 269 (1999) 536–553, http://dx.doi.org/10.1016/S0378-4371(99)00183-1.
[42] D. Höhner, Experimentelle und numiersche Untersuchungen zum Einfluss von Partikelgeometrie auf das mechanische Verhalten von Schüttgütern mit Hilfe der Diskreten Elemente Methode, 2014.
[43] H. Kruggel-Emden, S. Wirtz, V. Scherer, An analytical solution of different configurations of the linear viscoelastic normal and frictional-elastic tangential contact model, Chem. Eng. Sci. 62 (2007) 6914–6926, http://dx.doi.org/10.1016/j.ces.2007.08.049.
[44] K. Vollmari, R. Jasevičius, H. Kruggel-Emden, Experimental and numerical study of fluidization and pressure drop of spherical and non-spherical particles in a model scale fluidized bed, Powder Technol. 291 (2016) 506–521, http://dx.doi.org/10.1016/j.powtec.2015.11.045.
[45] D. Höhner, S. Wirtz, V. Scherer, Experimental and numerical investigation on the influence of particle shape and shape approximation on hopper discharge using the discrete element method, Powder Technol. 235 (2013) 614–627, http://dx.doi.org/10.1016/j.powtec.2012.11.004.
[46] F. Sudbrock, E. Simsek, S. Rickelt, S. Wirtz, V. Scherer, Discrete element analysis of experiments on mixing and stoking of monodisperse spheres on a grate, Powder Technol. 208 (2011) 111–120, http://dx.doi.org/10.1016/j.powtec.2010.12.008.
[47] O. Udoudo, Modelling the Efficiency of an Automated Sensor-based Sorter, 2010 (http://bib.convdocs.org/docs/1/288/conv_1/file1.pdf).